Modeling Distortion in Multichannel Communication Systems

Khaled M. Gharaibeh, *Member, IEEE,* and Michael B. Steer, *Fellow, IEEE*

***Abstract*—A behavioral modeling technique suited to capturing the response of wide-band multifunctional and multichannel amplifiers is introduced. The technique is based on the three-box approximation of the Volterra model and takes into account the dependence of the amplifier characteristics on frequency. The model is coupled with a new nonlinear statistical analysis, which enables accurate estimation of intermodulation and cross-modulation distortions of multiple digitally modulated signals. The model parameters can be obtained using simple measurements.**

***Index Terms*—Behavioral modeling, code division multiple access (CDMA), cross-modulation distortion, multichannel, nonlinear systems, power amplifiers, statistical modeling.**

I. Introduction

MULTIFUNCTIONAL and multichannel RF front-ends offer advantages in terms of size, cost, and system flexibility. In a multichannel base station, for example, power amplification is achieved using wide-band amplifiers that process multiple channels using common hardware (see Fig. 1) [1]. The use of a multichannel amplifier results in better spectrum utilization than can be achieved with architectures based on processing the channels individually. However, multichannel amplifiers are difficult to design and complicated to model. Invariably input signals interact with amplifier nonlinearities to cause self-distortion and cross-modulation distortion that compromise performance at a level exceeding that expected from simple extrapolation of distortion with a single channel. With multiple digitally modulated input signals, the nonlinear behavior results in two main unwanted distortion components. The first is the spectral regrowth caused by intermodulation and cross-modulation mechanisms, which are manifested as a degradation of SNR and adjacent channel interference (ACI). The second is the spurious components that appear at intermodulation frequencies and result in interference with other channels within the same operating band. Therefore, wireless standards such as wide-band code division multiple access (WCDMA) set maximum limits on ACI and on spurious intermodulation interference [2] when using multicarrier base stations.

Modeling distortion in a multichannel power amplifier requires coupling of an appropriate behavioral model with a statistical analysis that enables development of the output spectrum. In [3]–[9], single-channel statistical analyses were presented. However, most of these assumed that a digitally modulated signal could be approximated either by a single tone or by a narrow-band Gaussian noise (NBGN) process in addition to using a memoryless polynomial to model nonlinearity. With these approximations, distortion cannot be accurately estimated in a multichannel environment. First, a multichannel amplifier, being wide-band, exhibits frequency-dependent behavior that renders single-tone characteristics inadequate to model nonlinearity as the AM–AM and AM–PM characteristics vary across the band, as shown in Fig. 2. This behavior is regarded as one manifestation of memory effects where the system response depends not only on the input power level, but also on its frequency. Second, the NBGN assumption is a rough characteri-

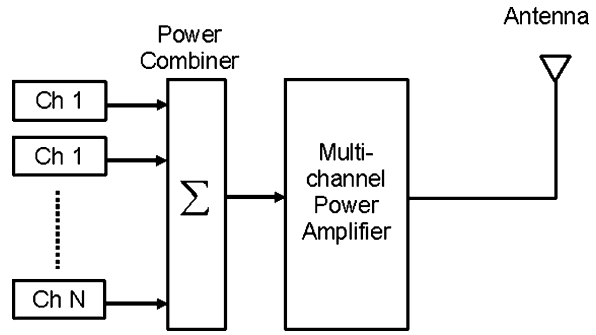

Fig. 1. Multichannel amplifier system.

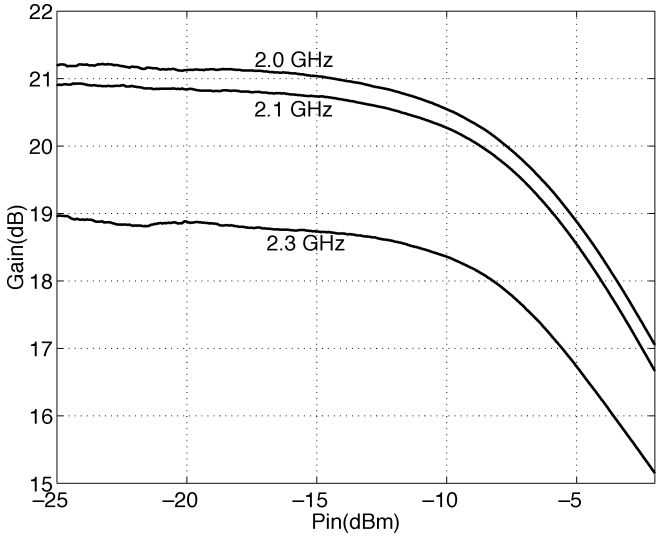

Fig. 2. Measured AM–AM characteristics of a microwave amplifier at various frequencies.

Manuscript received July 23, 2004; revised November 29, 2004. This work was supported by the National Science Foundation under Grant CCR-0120319 and by the U.S. Army Research Office as a Multidisciplinary University Research Initiative on Multifunctional Adaptive Radio Radar and Sensors under Grant DAAD19-0101-0496.

The authors are with the Department of Electrical and Computer Engineering, North Carolina State University, Raleigh, NC 27606 USA (e-mail: kmgharai@ncsu.edu; mbs@ncsu.edu).

Digital Object Identifier 10.1109/TMTT.2005.847064

zation of code-division multiple-access (CDMA) signals and it proves to be inadequate to model distortion in many situations (see [8]). In particular, the statistical properties of CDMA signals vary with the number of users, modulation, and data coding.

We have previously presented a statistical technique to estimate distortion in multichannel systems with the assumption that the channel characteristics are frequency independent [10]. In this case, a memoryless envelope model is adequate. In addition, the analysis does not capture the spurious components centered at intermodulation frequencies. The study presented here extends the analysis developed in [10] to model the interaction of multiple input signals in a multichannel power amplifier. The main contribution of this paper is in the development of a generalized autocorrelation and spectral analysis for multiple digitally modulated input signals. The analysis accurately characterizes the in-band intermodulation and cross-modulation distortions and also the spurious intermodulation spectra centered at the intermodulation frequencies of the input carriers. The analysis is coupled with the three-box behavioral model and, thus, it captures the variation of the nonlinear characteristics with frequency. Closed-form expressions for the output waveforms and their spectra at the complex envelope level are derived for multiple input signals. The simulations of multiple signals are done using WCDMA signal realizations and are verified by measurements of the output spectrum of an amplifier. There are two key results of this study. First, the analysis enables the simulation of the wide-band behavior of multichannel amplifiers using highly efficient computations. Second, the simplicity of the behavioral model and of its parameter-extraction procedure allows for its straightforward implementation in system simulators and development of intuitive understanding. Using experimental validation, it is shown that a behavioral model developed using simple measurements can be used in calculating distortion of multichannel digitally modulated signals.

II. Three-Box Approximation of Volterra Series

Various models based on simplifications of Volterra analysis have been developed that are easier to extract. Based on an established theory by Korenberg [11], [12], block models have been developed where a nonlinear system is represented by cascades of alternating linear and nonlinear elements. The three-box model belongs to this category of nonlinear models and takes the following form of the Volterra transfer function [11]:

$$H_n(f_1,\ldots,f_n) = a_n H_1(f_1)\ldots H_1(f_n)H_2(f_1+\ldots+f_n). \tag{1}$$

This form of the Volterra transfer function provides a considerable simplification of the analysis (compared to the general form) since it can be realized by the models shown in Fig. 3. This structure represents the nonlinear system by a cascade of linear operations that represents the finite memory of the system and a zero-memory nonlinearity. The three-box model is usually called the Wiener–Hammerstein model and is used to model a wide variety of nonlinear systems [12]–[16].

For nonlinear amplifiers, the three-box approximation of the Volterra model, despite its simplicity, captures memory effects

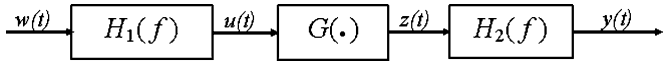

Fig. 3. Three-box approximation of the Volterra model.

that are manifested as multiple AM–AM curves at different frequencies, but have the same shape. If the nonlinear characteristics have different shapes, then the system cannot be modeled by the three-box model. The origins of these dissimilar nonlinear characteristics are certain memory effects caused by various phenomena such as the nonlinear parasitic capacitances of the nonlinear device, baseband conversion effects, and thermal effects. In this case, the model can be improved by considering more sophisticated structures (see [17]–[20]).

III. Multichannel Analysis Using the Three-Box Model

The three-box model shown in Fig. 3 consists of three major blocks, which are: 1) an input linear time invariant (LTI) filter with frequency response $H_1(f)$; 2) a static nonlinearity G; and 3) an output LTI filter with a frequency response $H_2(f)$. The static nonlinearity is described by the power series

$$z(t) = \sum_{n=0}^{N} a_n u^n(t)$$

where N is the maximum order nonlinearity. The model in this form was investigated in [17] and [18] and shown to adequately model the memory effect of a nonlinear amplifier where time-domain measurements were used to extract its parameters. Now consider a multichannel input signal $w(t)$ consisting of the sum of K modulated carriers and applied to the nonlinear amplifier so that

$$w(t) = \sum_{k=1}^{K} w_k(t).$$

Here, the signal $w_k(t)$ is a modulated RF carrier with center frequency ξ_k. The signal $u(t)$ at the output of the input filter can be written as a convolution of the input signal with the input filter impulse response as

$$u(t) = \int_{-\infty}^{\infty} h_1(\lambda)w(t-\lambda)d\lambda = \sum_{k=1}^{K} u_k(t)$$

where $h_1(t)$ is the impulse response of the input filter and

$$u_k(t) = \int_{-\infty}^{\infty} h_1(\lambda)w_k(t-\lambda)d\lambda.$$

The output of the nonlinear block is then

$$z(t) = \sum_{n=0}^{N} z_n(t)$$

where

$$z_n(t) = a_n \left(\sum_{k=1}^{K} u_k(t)\right)^n \tag{2}$$

is the nth-order nonlinear response. Finally, the total output of the model is

$$y(t) = \int_{-\infty}^{\infty} h_2(\lambda) z(t-\lambda) d\lambda = \sum_{n=1}^{N} \int_{-\infty}^{\infty} h_2(\lambda) z_n(t-\lambda) d\lambda \tag{3}$$

where $h_2(t)$ is the impulse response of the output filter.

In order to estimate distortion (particularly cross-modulation) introduced by the interaction of multiple signals, a closed-form expression for the output waveform at a particular frequency in complex envelope form is derived. The input to the nonlinear block $u_k(t)$ can be written in complex form as

$$\tilde{u}_k(t) = \int_{-\infty}^{\infty} \tilde{h}_{1;\xi_k}(\lambda) \tilde{w}_k(t-\lambda) d\lambda$$

where $\tilde{h}_{1;\xi_k}(t)$ is the baseband equivalent impulse response of the input filter with respect to frequency ξ_k and $\tilde{w}_k(t)$ is the complex envelope of the input signal $w_k(t)$. Hence, the total input to the nonlinear block can be written as a complex conjugate pair as

$$u(t) = \sum_{k=-K}^{K} \frac{1}{2} \tilde{u}_k(t) e^{j2\pi\xi_k t}$$

where the minus sign notation indicates complex conjugation so that $\tilde{u}_{-k} = \tilde{u}_k^*, \xi_{-k} = -\xi_k$. Following the analyses presented in [21]–[23], the nth-order output of the nonlinear block becomes

$$\begin{aligned} z_n(t) &= \frac{a_n}{2^n} \left(\sum_{k=-K}^{K} \tilde{u}_k(t) e^{j2\pi\xi_k t} \right)^n \\ &= \frac{a_n}{2^n} \sum_{k_1=-K}^{K} \cdots \sum_{k_n=-K}^{K} \prod_{i=1}^{n} \tilde{u}_{k_i}(t) e^{j2\pi\xi_{k_i} t} \\ &= \frac{a_n}{2^n} \sum_{k_1=-K}^{K} \cdots \sum_{k_n=-K}^{K} A(t) e^{j2\pi(\xi_{k_1}+\ldots+\xi_{k_n})t} \end{aligned} \tag{4}$$

where $A(t) = \prod_{i=1}^{n} \tilde{u}_{k_i}(t)$. The output $y(t)$ consists of components centered at all the intermodulation frequencies that result from the permutations of the input carrier frequencies represented by the frequency vector $(\xi_{k_1}, \ldots, \xi_{k_n})$. Therefore, the component of $z_n(t)$ centered at frequency $\xi = \xi_{k_1} + \ldots + \xi_{k_n}$ due to the intermodulation of input components (centered at the frequency vector $(\xi_{k_1}, \ldots, \xi_{k_n})$) can be expressed as [21]

$$\begin{aligned} z_{n,\xi}(t) = \sum_{n_{-K}\xi_k+\ldots n_K\xi_k=\xi} & \frac{a_n}{2^n} \binom{n}{n_{-K}, \ldots, n_K} \\ & \times \left(A(t) e^{j2\pi\xi t} + A^*(t) e^{-j2\pi\xi t} \right) \end{aligned}$$

where

$$\binom{n}{n_{-K}, \ldots, n_K} = \frac{n!}{n_K! \ldots n_{-K}!}$$

is the multinomial coefficient. Thus, the complex envelope of the output signal at the output of the nonlinear block and in the vicinity of a frequency ξ is

$$\tilde{z}_{n,\xi}(t) = \sum_{\xi_{k_1}+\ldots+\xi_{k_n}=\xi} \frac{a_n}{2^{n-1}} \binom{n}{n_{-K}, \ldots, n_K} A(t) \tag{5}$$

where $\xi = \sum_{k=-K}^{K} n_k \xi_k = \sum_{i=1}^{n} \xi_{k_i}$ and $\sum_{k=-K}^{K} n_k = n$. The complex envelope of the output $y(t)$ can now be written in complex envelope form as

$$\tilde{y}_\xi(t) = \sum_{n=1}^{N} \int_{-\infty}^{\infty} \tilde{h}_{2;\xi}(\lambda) \tilde{z}_{n,\xi}(t)(t-\lambda) d\lambda \tag{6}$$

where $\tilde{h}_{2;\xi}(t)$ is the baseband equivalent impulse response of the output filter with respect to frequency ξ. This expression enables the complex envelope of the output waveform to be related to the complex envelope of the input waveforms. In addition, this expression enables cross-modulation to be distinguished from intermodulation, as will be seen in Section III-A.

The development up to this point applies for an arbitrary number of channels, i.e., values of K. In the remainder of this section, we will consider two particular cases. Closed forms for the output waveform are developed when a single channel is input $(K = 1)$ and with two-channel input $(K = 2)$.

A. Single Channel

Consider the case where the input consists of a single narrowband signal $K = 1$ with carrier frequency ξ_1. The output complex envelope at the fundamental frequency ξ_1 is then, from (5),

$$\tilde{z}_{n,\xi_1}(t) = \sum_{n_{-1}+n_1=n} \frac{a_n}{2^{n-1}} \binom{n}{n_{-1}, n_1} \tilde{w}_{-1}^{n_{-1}} \tilde{w}_1^{n_1}(t). \tag{7}$$

Following [21], the contributing frequency vectors at frequency ξ_1, are all permutations of the vector $(\xi_1, \xi_1, -\xi_1)$ for $n = 3$, $(\xi_1, \xi_1, \xi_1, -\xi_1, -\xi_1)$ for $n = 5$, and so on. Therefore, $n_{-1} = (n-1)/2$, $n_1 = (n+1)/2$, and, thus, (7) becomes

$$\tilde{z}_{\xi_1}(t) = \sum_{n=1}^{N} b_n \tilde{u}_{-1}^{\frac{n-1}{2}} \tilde{u}_1^{\frac{n+1}{2}} \tag{8}$$

where

$$b_n = \frac{a_n}{2^{n-1}} \binom{n}{\frac{n-1}{2}, \frac{n+1}{2}}. \tag{9}$$

The interpretation of this result is as follows. In a single-channel system, the complex envelope of the nth-order output signal $\tilde{y}_{\xi_1}(t)$ centered at the carrier frequency ξ_1 is obtained from the complex envelope of the input signal given the nonlinear behavioral model (described by the power series coefficients and filter impulse responses) and applying (6). In the case of discrete tones, this expression represents the gain compression characteristic. The output complex envelope at any of the harmonics can also be derived in compact form, as in (8), using the appropriate frequency vectors.

B. Two Channels

A two-channel input ($K = 2$) will now be considered. The two channels are described by their complex envelopes $\tilde{u}_1(t)$ and $\tilde{u}_2(t)$ (at the output of the input filter) with respect to the frequencies ξ_1 and ξ_2, respectively. First, an expression for gain compression and gain saturation will be obtained by deriving the output envelope response centered at one of the carriers. Following a similar approach to that used above, the complex envelope of the output waveform at the first carrier (ξ_1) is

$$\tilde{z}_{n,\xi_1}(t) = \sum_{n_{-2}+n_{-1}+n_1+n_2=n} \frac{a_n}{2^{n-1}} \binom{n}{n_{-2}, n_{-1}, n_1, n_2} \times \tilde{u}_{-2}^{n_{-2}} \tilde{u}_{-1}^{n_{-1}} \tilde{u}_1^{n_1} \tilde{u}_2^{n_2}. \quad (10)$$

Again, following [21], the contributing vectors at frequency ξ_1 are all permutations of the vectors $(\xi_1, \xi_1, -\xi_1)$ and $(\xi_1, \xi_2, -\xi_2)$ for $n = 3$, vectors $(\xi_1, \xi_1, \xi_1, -\xi_1, -\xi_1)$, $(\xi_1, \xi_1, -\xi_1, \xi_2, -\xi_2)$, and $(\xi_1, \xi_2, \xi_2, -\xi_2, -\xi_2)$ for $n = 5$, and so on. By induction, $n_{-2} = l$, $n_{-1} = ((n-1)/2) - l$, $n_1 = ((n+1)/2) - l$, $n_2 = l$, and, hence, (10), can be written as the sum of the contributions defined by each of the above frequency vectors as

$$\tilde{z}_{\xi_1}(t) = \sum_{n=1}^{N} \sum_{l=0}^{\frac{n-1}{2}} b_{n,l} \tilde{u}_{-2}^{l} \tilde{u}_{-1}^{\frac{n-1}{2}-l} \tilde{u}_1^{\frac{n+1}{2}-l} \tilde{u}_2^{l} \quad (11)$$

where

$$b_{n,l} = \frac{a_n}{2^{n-1}} \binom{n}{l, \frac{n-1}{2} - l, \frac{n+1}{2} - l, l}.$$

This expression captures gain compression—the effect on the output $\tilde{z}_{\xi_1}$ due to the level of the input $\tilde{u}_1$ centered at the same frequency ξ_1, and gain saturation—the effect on the output $\tilde{z}_{\xi_1}$ due to the level of the input $\tilde{u}_2$ in the other channel centered at ξ_2. Since the second channel is modulated, gain saturation manifests itself as cross-modulation.

The intermodulation products can be derived in the same way by describing the nonlinear components by their frequency vectors. The lower intermodulation component $\mathrm{IM3}_L$ is centered at frequency $(2\xi_1 - \xi_2)$ and the contributing vectors at frequency $2\xi_1 - \xi_2$ are all the permutations of the vector $(\xi_1, \xi_1, -\xi_2)$ for $n = 3$, vectors $(\xi_1, \xi_1, \xi_1, -\xi_1, -\xi_2)$ and $(\xi_1, \xi_1, -\xi_2, -\xi_2, \xi_2)$ for $n = 5$, and so on. By induction, $n_{-2} = l + 1$, $n_{-1} = ((n-3)/2) - l$, $n_1 = ((n+1)/2) - l$, $n_2 = l$. Thus, the output complex envelope centered at frequency $(2\xi_1 - \xi_2)$ is

$$\tilde{z}(t)_{2\xi_1-\xi_2} = \sum_{n=3}^{N} \sum_{l=0}^{\frac{n-3}{2}} b_{n,l} \tilde{u}_{-2}^{l+1} \tilde{u}_{-1}^{\frac{n-3}{2}-l} \tilde{u}_1^{\frac{n+1}{2}-l} \tilde{u}_2^{l} \quad (12)$$

and for the upper intermodulation component $\mathrm{IM3}_U$, the output complex envelope centered at frequency $(2\xi_2 - \xi_1)$ is

$$\tilde{z}(t)_{2\xi_2-\xi_1} = \sum_{n=3}^{N} \sum_{l=0}^{\frac{n-3}{2}} b_{n,l} \tilde{u}_{-2}^{\frac{n-3}{2}-l} \tilde{u}_{-1}^{l+1} \tilde{u}_1^{l} \tilde{u}_2^{\frac{n+1}{2}-l} \quad (13)$$

where

$$b_{n,l} = \frac{a_n}{2^{n-1}} \binom{n}{\frac{n-3}{2} - l, l+1, l, \frac{n+1}{2} - l}.$$

The output $y(t)$ is then obtained for all the above output components after application of (6).

C. Summary

In Sections III-A and B, the input–output behavior of the nonlinear block was developed for one and two input channels. The full system response is obtained by incorporating the output filter response described by the convolution operations in (6). A memoryless system can be dealt with as a special case where the linear filters have an impulse response $h_1(\lambda) = h_2(\lambda) = \delta(\lambda)$ and, therefore, $\tilde{u}_k(t) = \tilde{w}_k(t)$ and the model reduces to a power series model.

What we have developed thus far is a complex envelope formulation for the output of the nonlinear amplifier. The complex envelope formulation is needed since all the simulations reported in this paper are performed at the envelope level. Envelope simulations are time efficient since the sampling frequency is commensurate with the bandwidth of the individual channels and do not depend on the frequency separation of channels.

IV. Distortion of Digitally Modulated Signal

In an earlier work [10], we showed that distortion in a multichannel system can be captured by developing the autocorrelation function at the output of the nonlinear system. The autocorrelation function is then used to develop the output spectrum from which distortion is estimated. The analysis was done for a memoryless system and was limited to modeling the in-band and out-of-band distortion in the vicinity of the channel of interest. Here, we use the multichannel model of the previous section and couple it with autocorrelation analysis to develop the output spectrum for a nonlinear system with memory at any intermodulation frequency. The frequency dependence of the behavioral model is captured by the linear filter responses.

First consider two modulated carriers $w_1(t)$ and $w_2(t)$ modulated at frequencies ξ_1 and ξ_2 where $\xi_2 > \xi_1$ and is applied at the input of the nonlinear amplifier. Referring to the three-box behavioral model in Fig. 3, the autocorrelation function of the envelope of the output waveform $z(t)$ is defined as

$$R_{\tilde{z}\tilde{z}}(\tau) = E\big[\tilde{z}(t)\tilde{z}^*(t+\tau)\big].$$

Now considering only the output component centered at frequency ξ_1, the autocorrelation function of the output of the second block is defined as

$$R_{\tilde{z}\tilde{z};\xi_1}(\tau) = E\big[\tilde{z}_{\xi_1}(t)\tilde{z}_{\xi_1}(t+\tau)\big]. \quad (14)$$

In [10], we showed that the output autocorrelation function is a function of the time shift (τ) provided that the two signals $\tilde{w}_1(t)$ and $\tilde{w}_2(t)$ are statistically independent and wide sense stationary (WSS) random processes. Note that the statistics of the modulated signal $z(t)$ are the same as the statistics of its

complex envelope since the carrier contains no information. Now, using (11), the autocorrelation function in (14) becomes

$$R_{\tilde{z}\tilde{z};\xi_1}(\tau)=\sum_{n=1}^{N}\sum_{m=1}^{N}\sum_{l=0}^{\frac{n-1}{2}}\sum_{k=0}^{\frac{m-1}{2}} b_{n,l}b^{*}_{m,k}R_{\tilde{u}_n\tilde{u}_m\tilde{u}_l\tilde{u}_k}(\tau) \quad (15)$$

where $R_{\tilde{u}_n\tilde{u}_m\tilde{u}_l\tilde{u}_k;\xi_1}(\tau)$ is as defined in (16) and (17) as follows:

$$\begin{aligned}
&R_{\tilde{u}_n\tilde{u}_m\tilde{u}_l\tilde{u}_k;\xi_1}(\tau)\\
&\quad=E\Bigg[\tilde{u}_1^{\frac{(n+1)}{2}-l}(t)\tilde{u}_{-1}^{\frac{(n-1)}{2}-l}(t)\tilde{u}_1^{\frac{(m-1)}{2}-k}(t+\tau)\\
&\qquad\times\tilde{u}_{-1}^{\frac{(m+1)}{2}-k}(t+\tau)\tilde{u}_2^{l}(t)\tilde{u}_{-2}^{l}(t)\tilde{u}_2^{k}(t+\tau)\\
&\qquad\times\tilde{u}_{-2}^{k}(t+\tau)\Bigg]\\
&\quad=R_{\tilde{w}_n\tilde{w}_m\tilde{w}_l\tilde{w}_k;\xi_1}(\tau)\left[\tilde{h}_{1;\xi_1}(0)\right]^{n+m-2l-2k}\\
&\qquad\times\left[\tilde{h}_{1;\xi_2}(0)\right]^{2l+2k} \qquad (16)\\
&R_{\tilde{w}_n\tilde{w}_m\tilde{w}_l\tilde{w}_k;\xi_1}(\tau)\\
&\quad=E\Bigg[\tilde{w}_1^{\frac{(n+1)}{2}-l}(t)\tilde{w}_{-1}^{\frac{(n-1)}{2}-l}(t)\tilde{w}_1^{\frac{(m-1)}{2}-k}(t+\tau)\\
&\qquad\times\tilde{w}_{-1}^{\frac{(m+1)}{2}-k}(t+\tau)\tilde{w}_2^{l}(t)\tilde{w}_{-2}^{l}(t)\\
&\qquad\times\tilde{w}_2^{k}(t+\tau)\tilde{w}_{-2}^{k}(t+\tau)\Bigg]. \qquad (17)
\end{aligned}$$

Note that (16) is derived assuming that the input filter response is constant within each signal bandwidth. The power spectral density (PSD) of the output signal $\tilde{z}_{\xi_1}(t)$ is obtained from the Fourier transform of the autocorrelation function as

$$S_{\tilde{z}\tilde{z};\xi_1}(f)=\sum_{n=1}^{N}\sum_{m=1}^{N}\sum_{l=0}^{\frac{n-1}{2}}\sum_{k=0}^{\frac{m-1}{2}} b_{n,l}b^{*}_{m,k}S_{\tilde{u};nmlk}(f) \quad (18)$$

where

$$S_{\tilde{u};nmlk}(f)=\left|\tilde{H}_{1;\xi_1}(0)\right|^{n+m-2l-2k}\left|\tilde{H}_{1;\xi_2}(0)\right|^{2l+2k}S_{\tilde{w};nmlk}(f)$$

and

$$S_{\tilde{w};nmlk;\xi_1}(f)=\int_{-\infty}^{\infty}R_{\tilde{w}_n\tilde{w}_m\tilde{w}_l\tilde{w}_k;\xi_1}(\tau)e^{-j\omega\tau d\tau}.$$

The PSD at the output of the system is

$$S_{\tilde{y}\tilde{y};\xi_1}(f)=\left|\tilde{H}_{2;\xi_1}(f)\right|^2S_{\tilde{z}\tilde{z};\xi_1}(f) \quad (19)$$

where $\tilde{H}_{1;\xi_i}(f)$ and $\tilde{H}_{2;\xi_i}(f)$ are the baseband equivalent transfer functions of the input and output filters with respect to frequency ξ_i.

The output autocorrelation function of the spurious intermodulation components can be developed in the same way. Therefore, for the upper and lower intermodulation components, using (12) and (13), the output autocorrelation function is

$$R_{\tilde{z}\tilde{z};\xi_{\mathrm{IM3}}}(\tau)=\sum_{n=3}^{N}\sum_{m=3}^{N}\sum_{l=0}^{\frac{n-3}{2}}\sum_{k=0}^{\frac{m-3}{2}} b_{n,l}b^{*}_{m,k}R_{\tilde{u}_n\tilde{u}_m\tilde{u}_l\tilde{u}_k}(\tau). \quad (20)$$

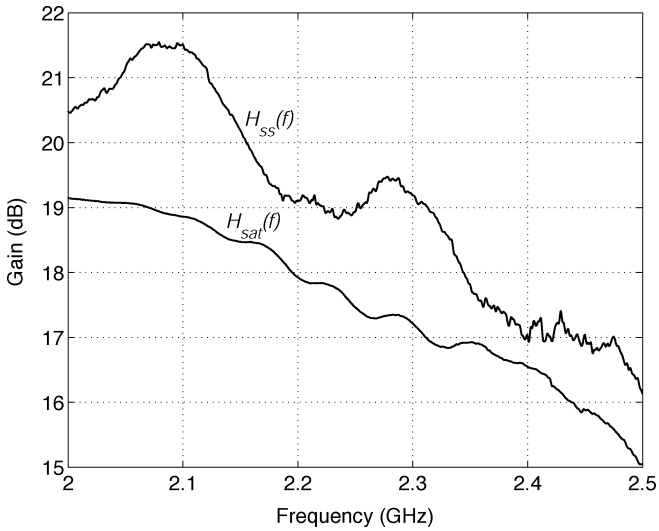

Fig. 4. Measured small- and large-signal frequency responses $H_{\mathrm{ss}}(f)$ and $H_{\mathrm{sat}}(f)$.

where ξ_{IM3} is the intermodulation frequency. Thus, for the upper intermodulation component (at $\xi_{\mathrm{IM3}U}=2\xi_2-\xi_1$), we have $R_{\tilde{u}_n\tilde{u}_m\tilde{u}_l\tilde{u}_k}(\tau)$, as defined in (21), and for the lower intermodulation component (at $\xi_{\mathrm{IM3}L}=2\xi_1-\xi_2$), as defined in (22). The output PSD of the intermodulation components is obtained in a similar way to (19) as follows:

$$\begin{aligned}
&R_{\tilde{u}_n\tilde{u}_m\tilde{u}_l\tilde{u}_k\xi_{\mathrm{IM3}U}}(\tau)\\
&\quad=E\Bigg[\tilde{u}_1^{l}(t)\tilde{u}_{-1}^{l+1}(t)\tilde{u}_1^{k+1}(t+\tau)\tilde{u}_{-1}^{k}(t+\tau)\\
&\qquad\times\tilde{u}_2^{\frac{(n+1)}{2}-l}(t)\tilde{u}_{-2}^{\frac{(n-3)}{2}-l}(t)\tilde{u}_2^{\frac{(m-3)}{2}-k}(t+\tau)\\
&\qquad\times\tilde{u}_{-2}^{\frac{(m+1)}{2}-k}(t+\tau)\Bigg] \qquad (21)\\
&R_{\tilde{u}_n\tilde{u}_m\tilde{u}_l\tilde{u}_k\xi_{\mathrm{IM3}L}}(\tau)\\
&\quad=E\Bigg[\tilde{u}_1^{\frac{(n+1)}{2}-l}(t)\tilde{u}_{-1}^{\frac{(n-3)}{2}-l}(t)\tilde{u}_1^{\frac{(m-3)}{2}-k}(t+\tau)\\
&\qquad\times\tilde{u}_{-1}^{\frac{(m+1)}{2}-k}(t+\tau)\tilde{u}_2^{l}(t)\tilde{u}_{-2}^{l+1}(t)\\
&\qquad\times\tilde{u}_2^{k+1}(t+\tau)\tilde{u}_{-2}^{k}(t+\tau)\Bigg]. \qquad (22)
\end{aligned}$$

The above results enable the autocorrelation function of the outputs centered at the carrier and intermodulation frequencies to be computed by combining the effects of the input and output filters, as well as the nonlinear block. Note that, with this formulation, the output spectrum is simply the spectrum of the memoryless nonlinearity multiplied by powers of the magnitude frequency response of the linear filters. This enables the easy implementation of the model in software where measured filter responses are multiplied by the spectrum generated from the Fourier transform of the autocorrelation function (17) computed for the particular digitally modulated signal(s).

Note that the output spectrum described by the summation (17) consists of the following output signal and distortion components:

- linear signal output;
- in-band gain compression (in-band means within each signal bandwidth);

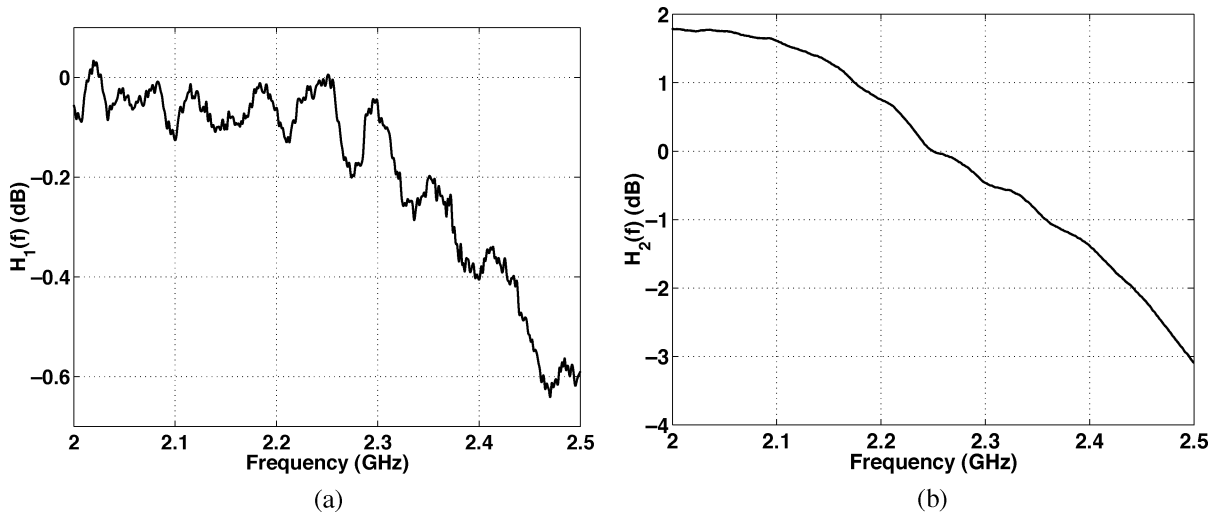

(a) (b)

Fig. 5. Normalized transfer characteristics of the input filter $H_1(f)$ and output filter $H_2(f)$.

- in-band spectral regrowth;
- out-of-band spectral regrowth which is responsible for ACI;
- in-band spectral regrowth from cross modulation;
- out-of-band spectral regrowth from cross modulation.

Finally, the spurious components centered at the intermodulation frequencies of the two carriers are described by the summation above (20). The distinction between intermodulation and cross-modulation terms is clear in this formulation since the cross-modulation is described by the cross terms (the terms that consist of the product of both signal envelopes). This enables different distortion terms to be identified and estimated.

V. Measurements and Simulation Results

Here, we first present the characterization of a wide-band amplifier that covers the band from 2.0 to 2.5 GHz. The amplifier considered has a gain of 21 dB, an output 1-dB compression point of 11 dBm, and an output third-order intercept (OIP3) of 18 dBm, all at 2.25 GHz, which is the middle of the operating band of the amplifier. The amplifier exhibits similar shapes of the AM–AM characteristics (shown in Fig. 2) at different frequencies across the band. The self-similar AM–AM characteristics at various frequencies indicate that the nonlinear reactive (i.e., frequency dependent) effects are insignificant and, thus, the amplifier is a good candidate for the three-box approximation of the Volterra model. The measurements presented here were done using the Agilent 8510B vector network analyzer (VNA), E4438C vector signal generator, and E4445A spectrum analyzer.

A. Model Parameters

Parameter extraction of the three-box model has been extensively investigated [17], [18], [24], [25]. Here, the simplified intuitive approach presented in [24] is followed. The system model (Fig. 3) consists of an LTI input filter, a static nonlinearity, and an LTI output filter. Following [24], the transfer functions of the linear filters are obtained by measuring the gain characteristics at saturation $H_{\rm sat}(f)$ (e.g., at the 1-dB compression point), and measuring the small-signal linear frequency response $H_{\rm ss}(f)$. The model parameters were extracted using a VNA as follows. The transfer functions $H_{\rm ss}(f)$ and $H_{\rm sat}(f)$ were obtained from S_{21} of the amplifier at low power level (-20 dBm) and at the 1-dB compression point (-8-dBm input power approximately) (see Fig. 4). The transfer functions of the linear filters $H_1(f)$ and $H_2(f)$ were computed from the measured filter transfer functions according to [24] and as follows: the transfer function of the pre-filter is given by

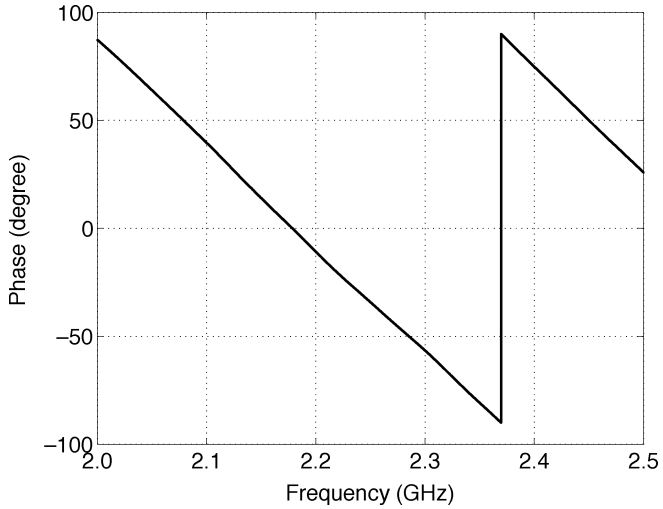

Fig. 6. Phase response of $H_{\rm ss}(f)$.

$$H_1(f) = \frac{H_{\rm ss}(f)}{G_{\rm ss}\,|H_{\rm sat}(f)|} \tag{23}$$

and the post-filter transfer function is given by

$$H_2(f) = \frac{|H_{\rm sat}(f)|}{|G_{\rm sat}|} \tag{24}$$

where $H_{\rm ss}(f)$ is the measured small-signal transfer function, $H_{\rm sat}(f)$ is the measured large-signal transfer function, and $G_{\rm ss} = |H_{\rm ss}(f_{\rm ref})|$ and $G_{\rm sat} = |H_{\rm sat}(f_{\rm ref})|$ are the small-signal gain and 1-dB compression gain at the reference frequency. The normalization of the filter responses is included in the memoryless nonlinearity. The filter responses are shown in Fig. 5 where

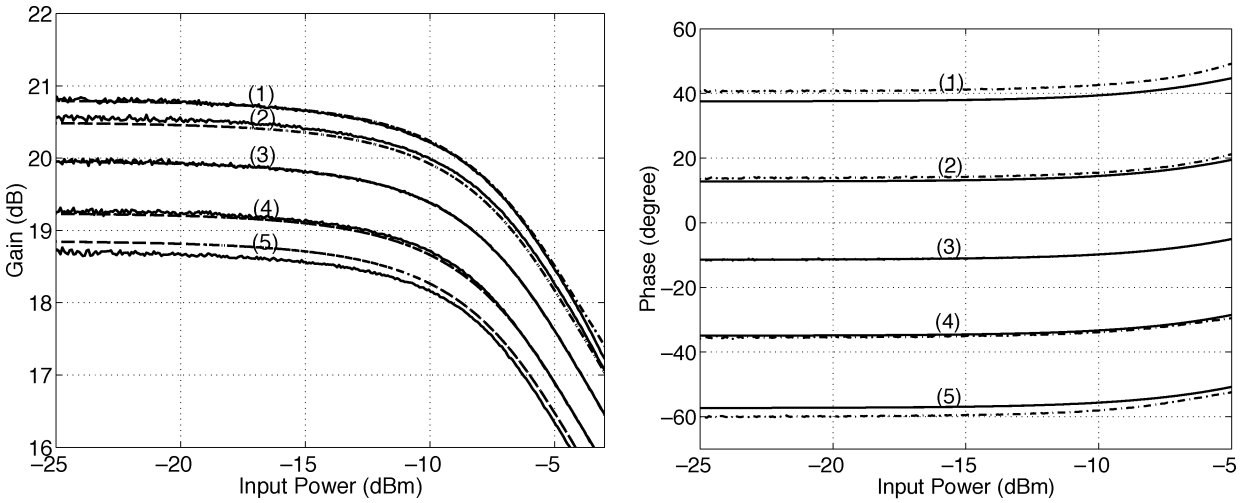

Fig. 7. Measured and predicted amplifier characteristics. (a) AM–AM and (b) AM–PM characteristics. Numerals indicate various frequencies: (1) $f_1 = 2.1$ GHz, (2) $f_2 = 2.15$ GHz, (3) $f_3 = 2.2$ GHz, (4) $f_{\rm ref} = 2.25$ GHz, and (5) $f_4 = 2.3$ GHz. The solid lines are measurements and the broken lines are predicted by using the three-box model.

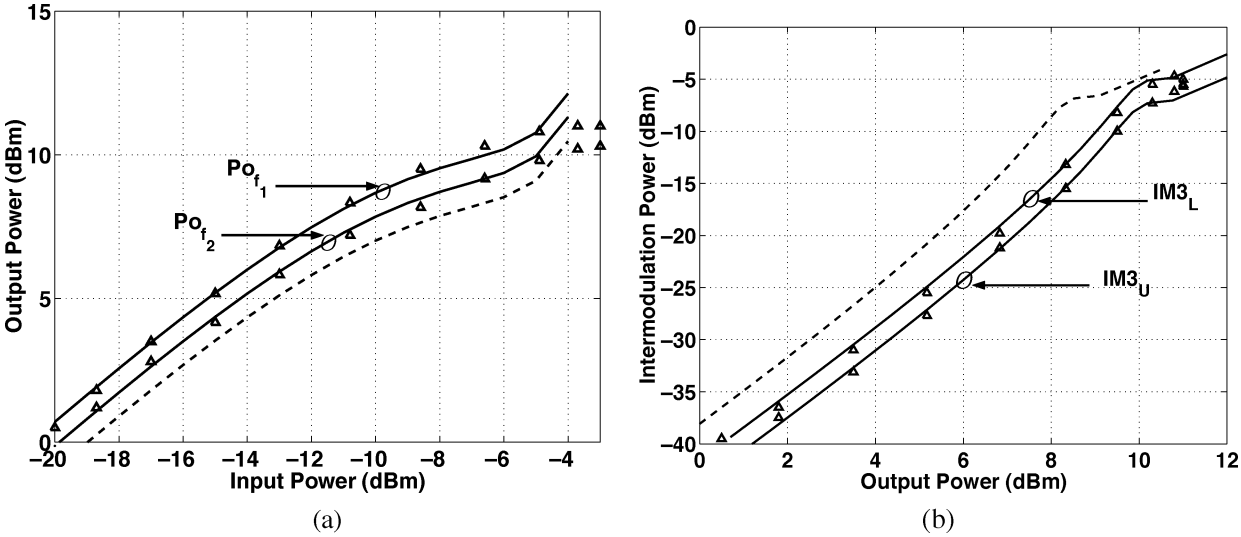

Fig. 8. Two-tone test results. (a) Output power with $f_1 = 2.1$ GHz and $f_2 = 2.2$ GHz. (b) Upper intermodulation component power level $(\mathrm{IM3}_U)$ and lower intermodulation component power level $(\mathrm{IM3}_L)$. Solid lines are simulated using the three-box model, broken line are simulated using the memoryless model, and $\triangle$ are measured results.

$f_{\rm ref} = 2250$ GHz. One of the assumptions behind the model extraction procedure is that the phase-frequency response is linear. This response is shown in Fig. 6 for the amplifier under test where it is seen that it is indeed linear across the band.

The static nonlinearity, the middle block in Fig. 3, is extracted as the measured single-tone AM–AM and AM–PM characteristics taken at a reference carrier frequency $f_{\rm ref}$. The required input–output characteristics of the nonlinear block are the memoryless nonlinear gain characteristics (instantaneous response) given by (8). The reference AM–AM and AM–PM characteristics are chosen to be measured at the middle frequency of the band of interest. The choice of the reference is arbitrary when the phase-frequency response is linear. The coefficients of the reference static nonlinearity were obtained by measuring the AM–AM and AM–PM characteristics at the reference frequency. A polynomial of order 5 was fitted to the complex data using classical least squares polynomial fitting and a set of envelope coefficients (b_n) was obtained. Since the envelop characteristics have odd symmetry, only odd-order envelope coefficients

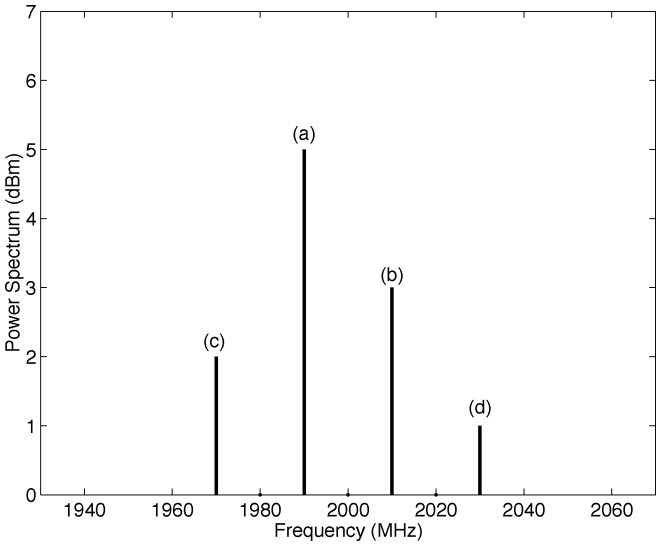

Fig. 9. Spectrum at the output of the amplifier with two WCDMA channels (a) and (b) applied.

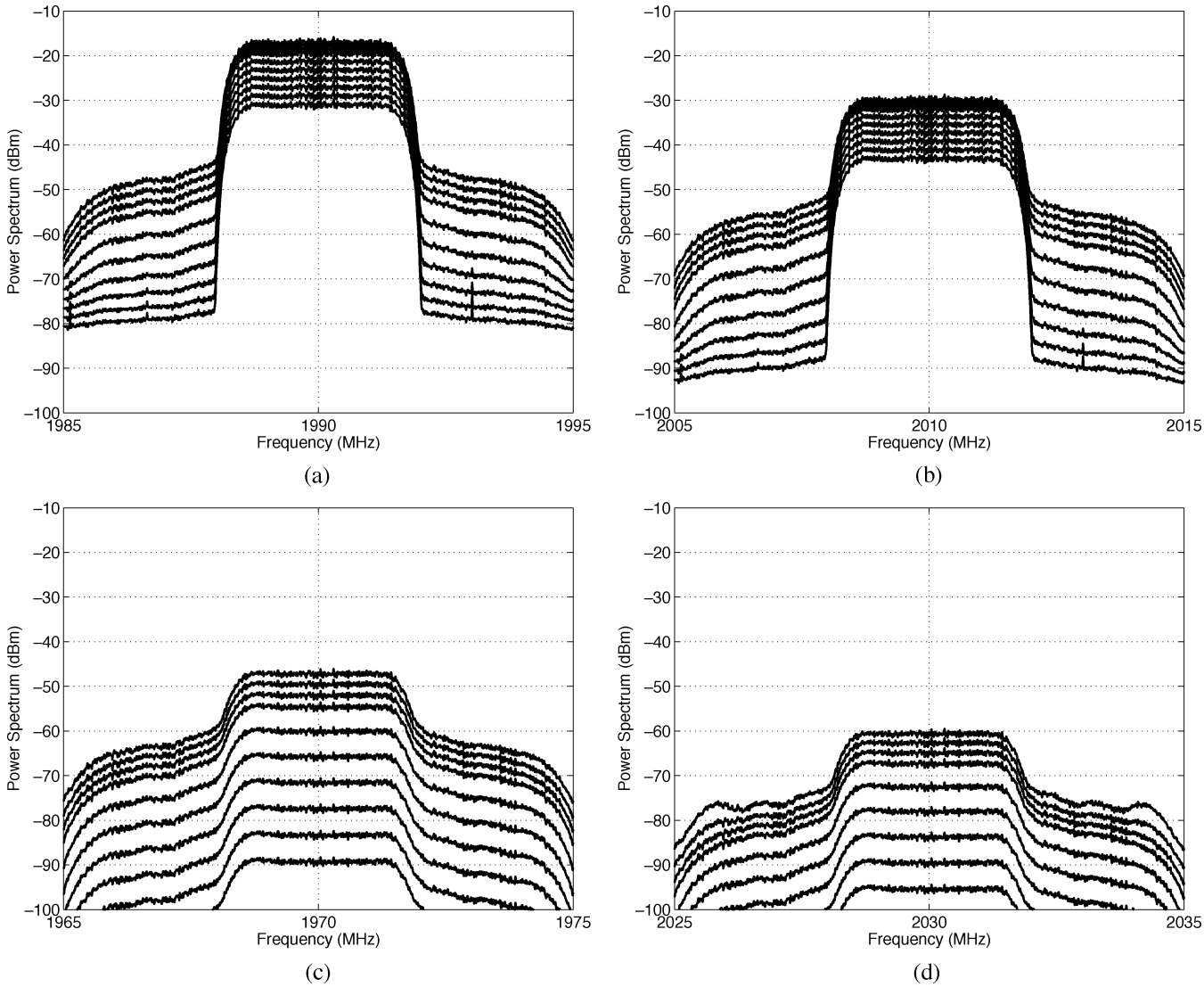

Fig. 10. Simulated output spectrum. (a) First WCDMA channel. (b) Second WCDMA channel. (c) Lower intermodulation component. (d) Upper intermodulation component. Shown are expansions of the corresponding components (a)–(d) of the broad spectrum shown in Fig. 9 and at different power levels.

can be obtained from measurements. The odd-order instantaneous coefficients a_n can then be developed from their envelope counterparts (b_n) using (9). Fortunately, only the odd-order components contribute to intermodulation and cross-modulation components that lie inside the bandwidth of the input signals, as shown in Section III.

The three-box model combines the frequency-dependent characteristics of the linear filters and the static nonlinearity to predict the overall amplifier response. The predicted single-tone response obtained using the three-box model is compared to the measured response in Fig. 7 at various power levels and across the band. Thus, the three-box model is seen to capture the single-tone behavior of the amplifier and should be entirely satisfactory when used to characterize the multichannel response of the amplifier. Sections V-B and C demonstrate that this is so for multitone and with multiple digitally modulated signals.

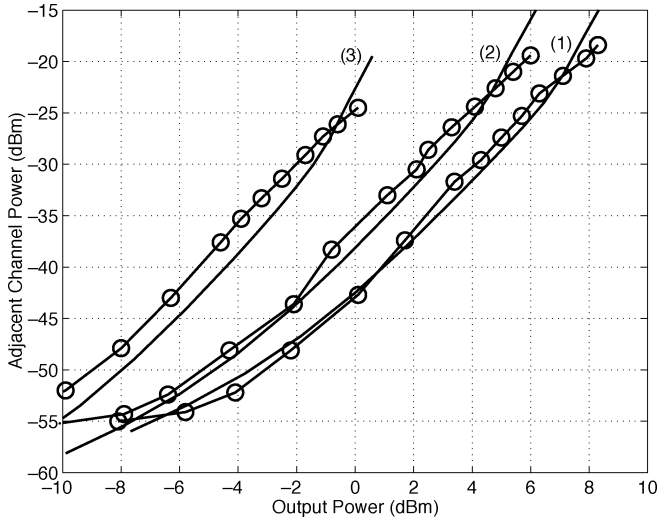

Fig. 11. ACP at the second carrier with the first carrier held at: (1) 3, (2) 6, and (3) 12 dB above the power of the second carrier. Solid: simulated. ∘: measured.

B. Two-Tone Testing With Wide Frequency Separation

In order to investigate the validity of the three-box model for multiple tones, a two-tone test was performed with wide frequency separation. The amplifier response to an input that consists of two equal amplitude tones centered at 2.1 and 2.2 GHz

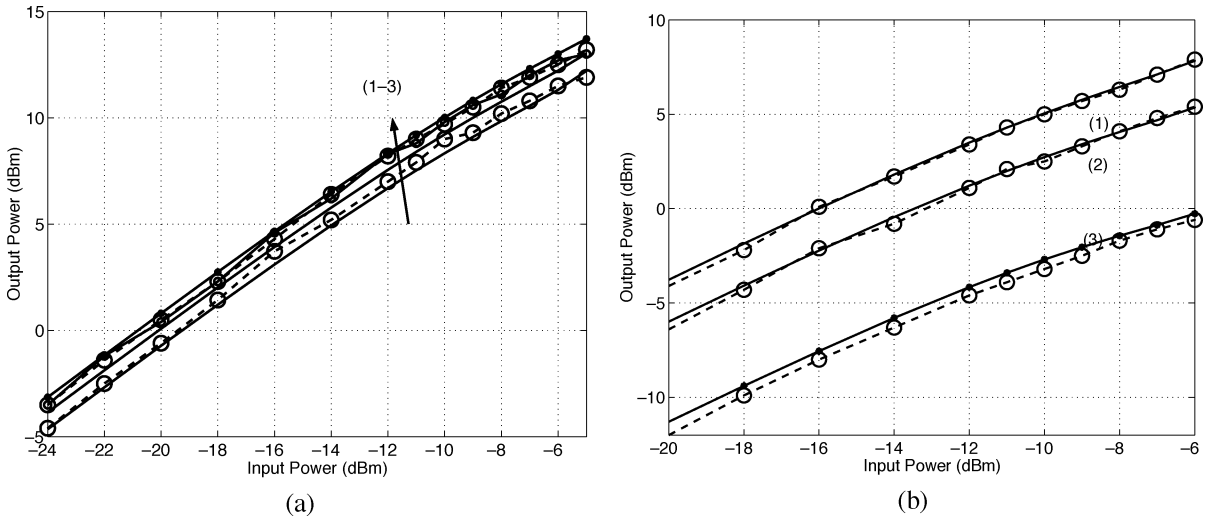

Fig. 12. Output power versus input power at: (a) the first carrier and (b) second carrier with the first carrier held at: (1) 3, (2) 6, and (3) 12 dB above the power of the second carrier. Solid: simulated. o: measured.

was measured. The frequency separation was chosen so that the asymmetry in the levels of the upper and lower intermodulation components due to memory effects is evident. Both being less than $f_{\rm ref}$ is a further test of the model. Fig. 8 presents the gain characteristics and intermodulation components (IM3) levels predicted by the three-box model and the memoryless model (with the filter responses excluded, $H_1(f) = H_2(f) = 1$). A good agreement between the measured and simulated values is seen when the three-box model is used. The frequency dependence evident in the measurements is, of course, not captured by the memoryless model.

The asymmetry in the upper and lower intermodulation products in this case is due to the variation of the frequency response of the amplifier with frequency. This figure shows a difference of 2 dB between the two intermodulation components, which the model predicts accurately. At high input powers (Fig. 8), discrepancies are evident between the measured and calculated responses. These discrepancies are particularly evident above -4-dBm input power corresponding to gain compression of 4 dB and more. The model evidently breaks down at these levels as the power series that captures the nonlinear behavior was fitted using single-tone measurements. While the single tone-measurements captured gain compression at the 4-dB level, the large peak-to-average ratio (PAR) of the two-tone test $(\mathrm{PAR} = 6\ \mathrm{dB})$ results in much larger signal excursions for the same compression level and, thus, the power series nonlinear model breaks down. This is exaggerated as power series extrapolate the asymptotic response of a limiting amplifier poorly.

C. WCDMA Signal Distortion

Here, it will be demonstrated that the statistical model developed in Section IV using the three-box model accurately captures distortion of multiple digitally modulated signals. In particular, the case where two WCDMA channels are input to the amplifier and distortion at the output is experimentally characterized and compared with simulations using the behavioral model. Two forward-link WCDMA test signals, which have a nominal bandwidth of 3.84 MHz, were used. The autocorrelation functions derived in (15) and (20) were computed using CDMA signal realization and the behavioral model developed in Section V-A. The PSD of the output was computed from the fast Fourier transform (FFT) of the autocorrelation function where gain compression, spectral regrowth, and the spurious intermodulation components were estimated. The two channels are centered at 1990 and 2010 MHz and the calculated spectrum at the output of the amplifier is shown in Fig. 9. At this scale, only the carriers of the channels are seen at: (a) 1990 MHz and (b) 2010 MHz, and intermodulation components at: (c) 1970 MHz (the lower intermodulation component) and (d) 2030 MHz (the upper intermodulation component). This is just the spectrum that would be observed with two tones—unmodulated sine waves—exciting the amplifier. The digitally modulated structure of the channels can be seen in Fig. 10 where the components of the spectrum are expanded and the parts of the figure are as indicated in Fig. 9. Fig. 10 shows the simulated output spectra with the total input power level varies -25 to -5 dBm and the channel at 2010 MHz held at 12 dB below the power of the channel at 1990 MHz. Note that the shape of the intermodulation components depends on the correlation between the data in the two channels. The spectra shown in Fig. 10 are for two similar data channels. The predictions of the model were verified using adjacent channel power (ACP) and the power in the intermodulation components. Fig. 11 shows the measured ACP at the second carrier (2010 MHz), Fig. 12 shows the power in the intermodulation components at 1970 and 2030 MHz, and Fig. 13 shows output power versus input power compared to that simulated using the statistical model. The ACP was measured in a 3.84-MHz bandwidth at a 5-MHz offset from carrier and the intermodulation components were measured in a 3.84-MHz bandwidth around the intermodulation frequencies. The total input power was varied from -25 to -5 dBm and the power of the first channel was held at 3, 6, and 12 dB above the second channel. This is indicated by the different curves for ACP and the intermodulation components in Figs. 11–13. The simulations where done using the three-box

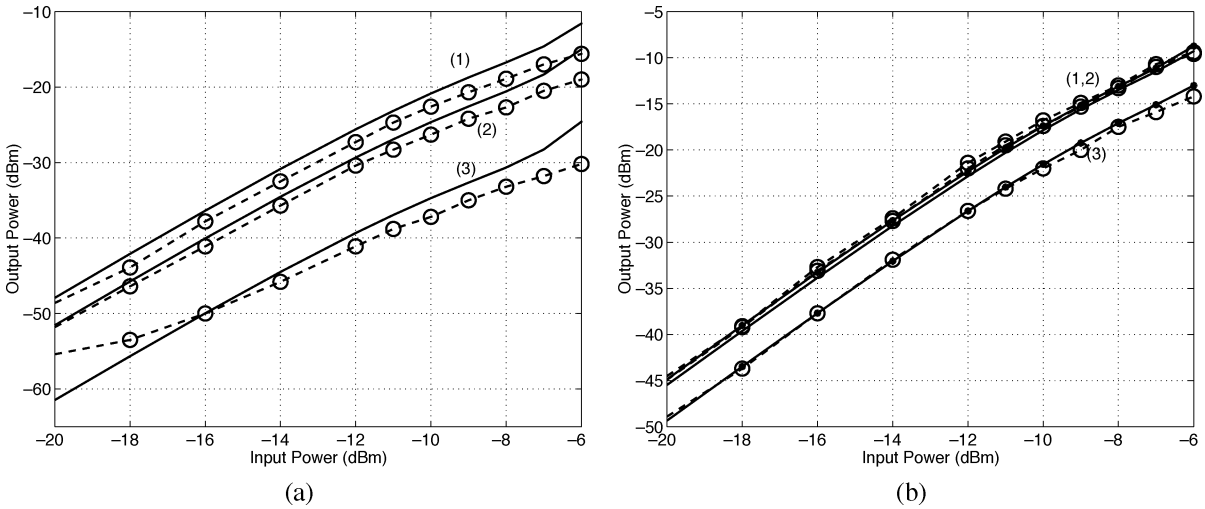

Fig. 13. (a) Power in the upper intermodulation components and (b) the lower intermodulation components with the first carrier held at: (1) 3, (2) 6, and (3) 12 dB above the power of the second carrier. Solid: simulated. ∘: measured.

behavioral model with reference frequency $f_{\text{ref}} = 2250$ MHz. It is clear that the three-box model accurately predicts the ACP.

VI. Conclusion

A behavioral modeling technique for modeling the interaction of multiple digitally modulated signals in a multichannel RF system has been presented and verified. The new technique is based on the three-box approximation of the Volterra model, which captures the behavior of a nonlinear amplifier with self-similar shapes of the AM–AM characteristics at frequencies across the band of interest. The parameters of the three-box model were extracted using simple VNA measurements. The three-box model was used to develop a statistical analysis for multiple digitally modulated signals from which the output spectra can be developed. This enables the accurate estimation of intermodulation and cross-modulation distortions, which are of great concern in multichannel PA design. It has been shown that using the three-box model provides better accuracy in the estimation of distortion than does the memoryless model commonly used when only single-tone characterization is available. This is because the three-box model adequately captures the nonlinear behavior with multiple channels with significant frequency separation of the channels, as well as their power levels.

References

[1] P. B. Kenington, *High Linearity Amplifier Design*. Norwood, MA: Artech House, 2000.

[2] "Designing and testing 3GPP W-CDMA user equipment," Agilent Technol., Palo Alto, CA, Applicat. note 1356, 2003.

[3] K. Gard, H. Gutierrez, and M. B. Steer, "Characterization of spectral regrowth in microwave amplifiers based on the nonlinear transformation of a complex Gaussian process," *IEEE Trans. Microw. Theory Tech.*, vol. 47, no. 7, pp. 1059–1069, Jul. 1999.

[4] C. Liu, H. Xiao, Q. Wu, and F. Li, "Spectrum design of RF power amplifier for wireless communication systems," *IEEE Trans. Consum. Electron.*, vol. 48, no. 1, pp. 72–80, Feb. 2002.

[5] G. T. Zhou, "Analysis of spectral regrowth of weakly nonlinear power amplifiers," in *IEEE Acoustics, Speech, and Signal Processing Conf.*, vol. 5, Jun. 2000, pp. 2737–2740.

[6] T. S. Goh and R. D. Pollard, "ACPR prediction of CDMA systems through statistical behavioral modeling of power amplifiers with memory," in *Int. Comm. Conf.*, vol. 2, Nov. 2002, pp. 1189–1193.

[7] T. Wang and T. J. Brazil, "Using Volterra mapping based behavioral models to evaluate ACI and cross modulation in CDMA communication systems," in *High Frequency Postgraduate Student Colloq.*, Sep. 2000, pp. 102–108.

[8] V. Aparin, "Analysis of CDMA signal spectral regrowth and waveform quality," *IEEE Trans. Microw. Theory Tech.*, vol. 49, no. 12, pp. 2306–2314, Dec. 2001.

[9] W. Qiang, M. Testa, and R. Larkin, "Linear RF power amplifier design for CDMA signals," in *IEEE MTT-S Int. Microwave Symp. Dig.*, vol. 2, Jun. 1996, pp. 851–854.

[10] K. M. Gharaibeh and M. B. Steer, "Characterization of cross modulation in multichannel amplifiers using a statistically based behavioral modeling technique," *IEEE Trans. Microw. Theory Tech.*, vol. 51, no. 12, pp. 2434–2444, Dec. 2003.

[11] H. W. Chen, "Modeling and identification of parallel nonlinear systems: Structural classification and parameter estimation methods," *Proc. IEEE*, vol. 83, no. 1, pp. 39–66, Jan. 1995.

[12] M. Korenberg, "Parallel cascade identification and kernel estimation for nonlinear systems," *Ann. Biomed. Eng.*, vol. 19, pp. 429–455, 1991.

[13] M. Shcetzen, "Nonlinear system modeling based on the Wiener theory," *Proc. IEEE*, vol. 69, no. 12, pp. 1557–1573, Dec. 1981.

[14] J. Shi and H. H. Sun, "Nonlinear system identification for cascaded block model: An application to electrode polarization impedance," *IEEE Trans. Biomed. Eng.*, vol. 37, no. 6, pp. 574–587, Jun. 1990.

[15] P. Crama and J. Schoukens, "Initial estimates of Wiener and Hammerstein systems using multisine excitation," *IEEE Trans. Instrum. Meas.*, vol. 50, no. 6, pp. 1791–1795, Dec. 2001.

[16] D. T. Westwick and R. E. Kearney, "Identification of a Hammerstein model of the stretch reflex EMG using separable least squares," in *Proc. 22nd Annu. IEEE Engineering in Medicine and Biology Society*, vol. 3, Jul. 2000, pp. 1901–1904.

[17] C. P. Silva, A. A. Moulthrop, and M. S. Muha, "Polyspectral techniques for nonlinear system modeling and distortion compensation," in *3rd IEEE Vacuum Electronics Conf.*, Apr. 2002, pp. 314–315.

[18] M. S. Muha, C. J. Clark, A. A. Moulthrop, and C. P. Silva, "Validation of power amplifier nonlinear block models," in *IEEE MTT-S Int. Microwave Symp. Dig.*, vol. 2, Jun. 1999, pp. 759–762.

[19] H. Ku, M. D. McKinley, and J. S. Kenney, "Quantifying memory effects in RF power amplifiers," *IEEE Trans. Microw. Theory Tech.*, vol. 50, no. 12, pp. 2843–2849, Dec. 2002.

[20] J. C. Pedro, N. B. Carvalho, and P. M. Lavrador, "Modeling nonlinear behavior of bandpass memoryless and dynamic systems," in *IEEE MTT-S Int. Microwave Symp. Dig.*, Jun. 2003, pp. 2133–2136.

[21] J. W. Graham and L. Ehrmen, *Nonlinear System Modeling and Analysis With Application to Communication Receivers*. Rome, NY: Rome Air Developement Center, 1973.

[22] G. W. Rhyne, "Nonlinear analysis of microwave circuits," Ph.D. dissertation, Dept. Elect. Comput. Eng., North Carolina State Univ., Raleigh, NC, 1988.

[23] P. J. Lunsford II, "The frequency domain behavioral modeling and simulation of nonlinear analogue circuits and systems," Ph.D. dissertation, Dept. Elect. Comput. Eng., North Carolina State Univ., Raleigh, NC, 1993.
[24] M. Jeruchim, P. Balaban, and S. Shanmugan, *Simulation of Communication Systems*. Norwell, MA: Kluwer, 2000.
[25] C. J. Clark, C. P. Silva, A. A. Moulthrop, and M. S. Muha, "Power-amplifier characterization using a two-tone measurement technique," *IEEE Trans. Microw. Theory Tech.*, vol. 50, no. 6, pp. 1590–1602, Jun. 2002.
[26] J. S. Bendat, *Nonlinear System Analysis and Identification*. New York: Wiley, 1990.

Khaled M. Gharaibeh (S'01–M'04) received the B.S. and M.S. degrees in electrical engineering from the Jordan University of Science and Technology, Irbid, Jordan, in 1995 and 1998, respectively, and the Ph.D. degree in electrical engineering from North Carolina State University, Raleigh, in 2004.

From 1996 to 2000, he was a Planning Engineer with Jordan Telecom, Amman, Jordan. Since January 2004, he has been a Research Associate Post Doc with the Department Electrical and Computer Engineering, North Carolina State University. His research interests are nonlinear system identification, behavioral modeling of nonlinear RF circuits and digital communications.

Dr. Gharaibeh is a member of Eta Kappa Nu.

Michael B. Steer (S'76–M'82–SM'90–F'99) received the B.E. and Ph.D. degrees in electrical engineering from the University of Queensland, Brisbane, Australia, in 1976 and 1983, respectively.

He is currently a Professor with the Department of Electrical and Computer Engineering, North Carolina State University, Raleigh. In 1999 and 2000, he was a Professor with the School of Electronic and Electrical Engineering, The University of Leeds, where he held the Chair in microwave and millimeter-wave electronics. He was also Director of the Institute of Microwaves and Photonics, The University of Leeds. He has authored approximately 300 publications on topics related to RF, microwave and millimeter-wave systems, high-speed digital design, and RF and microwave design methodology and circuit simulation. He coauthored *Foundations of Interconnect and Microstrip Design* (New York: Wiley, 2000).

Prof. Steer is active in the IEEE Microwave Theory and Techniques Society (IEEE MTT-S). In 1997, he was secretary of the IEEE MTT-S. From 1998 to 2000, he was an elected member of its Administrative Committee. He is the Editor-in-Chief of the IEEE TRANSACTIONS ON MICROWAVE THEORY AND TECHNIQUES (2003–2006). He was a 1987 Presidential Young Investigator (USA). In 1994 and 1996, he was the recipient of the Bronze Medallion presented by the Army Research Office for "Outstanding Scientific Accomplishment." He was also the recipient of the 2003 Alcoa Foundation Distinguished Research Award presented by North Carolina State University.